Predicting self-diffusion in metal oxides from first principles: The case of oxygen in tetragonal ZrO_2

Mostafa Youssef and Bilge Yildiz*

Laboratory for Electrochemical Interfaces, Department of Nuclear Science and Engineering, Massachusetts Institute of Technology, 77 Massachusetts Avenue, Cambridge, Massachusetts 02139, USA

(Received 9 August 2013; published 16 January 2014)

Theoretical prediction of self-diffusion in a metal oxide in a wide range of thermodynamic conditions has been a long-standing challenge. Here, we establish that combining the formation free energies and migration barriers of all charged oxygen defects as calculated by density functional theory, within the random-walk diffusion theory framework, is a viable approach to predicting oxygen self-diffusion in metal oxides. We demonstrate this approach on tetragonal ZrO_2 by calculating oxygen self-diffusivity as a function of temperature and oxygen partial pressure or, alternatively, temperature and off-stoichiometry. Arrhenius analysis on the isobaric (or constant off-stoichiometry) self-diffusivities yields a spectrum of effective activation barriers and prefactors. This provides reconciliation for the wide scatter in the experimentally determined activation barriers and prefactors for many oxides.

DOI: 10.1103/PhysRevB.89.024105 PACS number(s): 66.30.Dn, 66.30.H−

I. INTRODUCTION

Optimizing the performance of metal oxides in their applications requires a fundamental understanding of their point defect equilibria and migration kinetics.[1] Recently, we introduced a framework to predict point defect equilibria in a metal oxide in the limit of noninteracting defects.[2] The framework is informed by density functional theory (DFT) and takes into account finite temperature effects. In this paper, we extend this framework to account for defect diffusion kinetics as epitomized in the *self-diffusion coefficient*.

Self-diffusivities in metal oxides are critical to model processes such as corrosion, crystal growth, sintering, and diffusional creep.[3] Experimental determination of self-diffusivities and identifying the mediating defect is a challenging task, and for many oxides, there is no consensus either on the effective activation barriers or the mediating defect.[3,4] Theoretical work focused on computing the formation or migration energies of the defects or both.[4–6] However, extending the formation energies to defect concentrations as a function of thermodynamic conditions, which is nontrivial for a metal oxide,[2] and combining them with migration barriers to obtain self-diffusivities has not been accomplished satisfactorily. For example, earlier work had to assume the domination of a certain defect to compute self-diffusivities as a function of the concentration of that particular defect.[7] Recently, self-diffusivity due to neutral oxygen defects in SiO_2 was obtained starting from DFT calculations without prior assumptions about the predominant defect.[8] However, for most oxides, charged defects prevail, and their varying and competing concentrations as a function of temperature leads to phenomena such as the non-Arrhenius behavior on diffusivity isobars, which we demonstrate also in this paper. In Ref. 6, oxygen charged defects were included in computing the isothermal self-diffusivity of oxygen in ZnO. However, the resulting diffusivity was presented as a function of both oxygen and electron chemical potentials. Those results have some validity when the variation in electron chemical potential is due to dopants in dilute solid solutions. However, these two variables are in fact not independent for a fixed composition and at a fixed temperature. Resolving the dependence of electron chemical potential on temperature (T) and oxygen partial pressure (P_{O_2}) (Ref. 2) enables evaluating the diffusivity as a function of (T) and (P_{O_2}), which are independent variables.

In this paper, we adopt tetragonal zirconia (T-ZrO_2) as a model system, whose defect thermodynamics were assessed in our recent work.[2] We focus on the diffusion of oxygen, although the approach is also applicable to cation diffusion. Without prior assumptions about the dominant defect, we employed random-walk diffusion theory to combine the herein-computed migration barriers of oxygen defects with their previously determined concentrations,[2] obtaining oxygen self-diffusivity as a function of T and P_{O_2}. To compare our results to experiments in which oxide off-stoichiometry was fixed,[9] we recast the calculated diffusivity in the form of a function of temperature and off-stoichiometry. By performing Arrhenius analysis on both the isobaric and the constant off-stoichiometry diffusivities, two spectra of effective activation barriers and prefactors emerge, providing an explanation for the wide scatter in effective activation energies and prefactors documented in the literature for many metal oxides.[4,6]

II. THEORETICAL AND COMPUTATIONAL APPROACH

From random-walk diffusion theory,[3,6] the one-dimensional self-diffusivity of a defect d, is given by

$$D = \frac{1}{2}[d]\sum_k \zeta_k \lambda_k^2 \Gamma_k^d, \tag{1}$$

where $[d]$ is the defect concentration, and the summation is taken over all the crystallographic directions k that have a nonzero projection on the one dimension under investigation. For each crystallographic direction k, ζ_k is its multiplicity, λ_k is the length of its projection on the one dimension of interest, and Γ_k^d is the jump frequency of the defect d in the direction k.

In a constant-volume ensemble, Γ_k^d is given by[10]

$$\Gamma_k^d = \upsilon_k^d \exp\left(\frac{-E_k^d}{k_B T}\right), \tag{2}$$

TABLE I. The calculated migration energy barriers (in eV) of oxygen defects in T-ZrO_2. The crystallographic directions and the jump distances are based on the perfect conventional unit cell. DFT results from Ref. 18 and classical pair potential calculations from Ref. 19 are shown for comparison. For V_O^x, barriers based on both the triplet (net spin $2\mu_B$) and the singlet ($0\mu_B$) saddle points are shown.

	Jump distance along the given crystallographic direction						
Defect	⟨100⟩ 2.64 Å	⟨001⟩ 2.65 Å	⟨110⟩ 3.64 Å	⟨$\bar{1}$10⟩ 3.64 Å	⟨101⟩ 3.30 Å	⟨$\bar{1}$01⟩ 4.13 Å	⟨111⟩ 4.51 Å
$V_O^{\bullet\bullet}$	0.38	0.58	2.64	3.82	4.32	1.79	3.70
$V_O^{\bullet\bullet}$ Ref. 18	0.22[a]	0.61					
$V_O^{\bullet\bullet}$ Ref. 19	0.27	0.26					
$V_O^x(2\mu_B)$	1.59	1.24	2.83	2.90	2.16	3.76	3.88
$V_O^x(0\mu_B)$	1.48	1.65	3.11	3.39	2.34	3.96	2.91
$V_O^x(0\mu_B)$ Ref. 18	1.35[a]	1.43					
		Interstitialcy (2.44 Å)				Interstitialcy (2.10 Å)	
O_i''		1.41				0.28	
O_i'' Ref. 19		1.50				0.40	

[a]In Ref. 18, these barriers were reported for the ⟨110⟩ direction of the primitive cell, which is equivalent to the ⟨100⟩ direction for the conventional one.

where k_B is the Boltzmann constant. For the defect d that jumps in direction k, υ_k^d and E_k^d are the attempt frequency and the migration energy barrier, respectively. The migration entropy is carried by the term υ_k^d, which is taken as 5 THz in this paper. By adopting the vectors [100], [010], [001] as a basis for the conventional unit cell of T-ZrO_2 and calculating D for each defect in the directions of the basis vectors, we obtained a diagonal diffusivity tensor (see the Supplemental Materials[11]). The trace of this tensor is the quasi-isotropic self-diffusion coefficient of the defect. By summing the self-diffusivities of all oxygen defects, we obtain the total oxygen self-diffusivity D_{tot}. Including correlation effects to obtain tracer diffusivity introduces a negligible correction[3,6] and is beyond the scope of this paper. In what follows, all diffusivities are understood as *self*.

In a metal oxide, the defect concentration depends on P_{O_2}, as does the defect self-diffusivity. In Ref. 2, we determined the P_{O_2} dependence of defect concentrations utilizing the charge neutrality condition. Here, we evaluated the migration barriers for oxygen defects and combined their concentrations and migration barriers as indicated in Eqs. (1) and (2). The oxygen defects considered are the doubly charged oxygen vacancy $V_O^{\bullet\bullet}$, the neutral oxygen vacancy V_O^x, and the doubly charged oxygen interstitial O_i''. The singly charged vacancy and interstitial were deemed disallowed by the negative U behavior, and the neutral oxygen interstitial O_i^x was found to have very low concentration; hence, these defects are not considered here.[2]

The migration barriers were calculated by the climbing image nudged elastic band method[12] using three to five intermediate images. DFT total energies were calculated using the projector-augmented plane wave method[13] as implemented in the Vienna *Ab initio* Simulation Package.[14] The standard Perdew-Burke-Ernzerhof[15] functional was used to treat the exchange-correlation interaction. Other details of the computational method are the same as in Ref. 2. The experimental[16] band gap of 4.2 eV was adopted in our calculation of defect concentrations because of better consistency with conductivity measurements in T-ZrO_2.[2,17]

III. RESULTS AND DISCUSSION

Table I summarizes the calculated migration barriers and the corresponding jump distances for all the oxygen vacancies and interstitials considered. In Fig. 1, we schematically depict representative migration pathways for the oxygen vacancy and the oxygen interstitial in the conventional unit cell of tetragonal ZrO_2. For $V_O^{\bullet\bullet}$ and V_O^x, we considered all the possible and distinct diffusive jumps within the conventional unit cell. Seven distinct jumps were identified, as shown in Table I. The DFT results of Eichler,[18] who considered the migration of $V_O^{\bullet\bullet}$ and V_O^x in ⟨100⟩ and ⟨001⟩ directions, are in agreement with our calculations, as shown in Table I. The classical pair potential predictions of Ref. 19 for the migration of $V_O^{\bullet\bullet}$ is also consistent with our computed barrier for this defect in ⟨100⟩. However, this classical potential underestimates the barrier in ⟨001⟩ to the extent that it predicts an isotropic diffusion in ⟨100⟩ and ⟨001⟩.

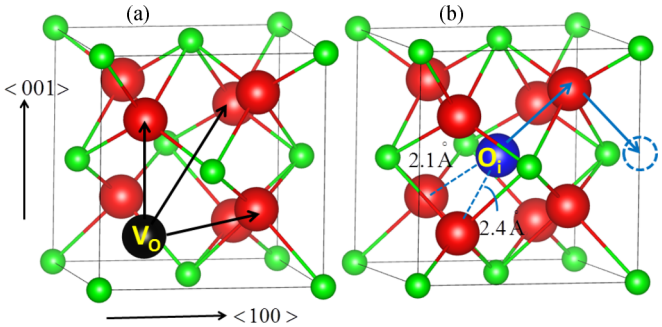

FIG. 1. (Color online) Schematic shows representative migration pathways for oxygen defects in tetragonal ZrO_2. Zirconium cations and oxygen anions are represented by green (small) and red (large) balls, respectively. (a) Three representative migration hops for an oxygen vacancy in ⟨001⟩, ⟨100⟩, and ⟨111⟩. (b) A representative interstitialcy migration hop for an oxygen interstitial originally located in an octahedral site in the conventional unit cell. Due to the tetragonal distortion of the oxygen columns, four lattice oxygen sites are at a distance of 2.44 Å from any octahedral site, whereas the other four are at a distance of 2.10 Å from the same site.

The V_O^x is an F-center with two electrons localized on the vacant site.[2,18] Its ground state is singlet. The diffusive jump of an F-center involves two simultaneous events, namely, the jump of a neighboring oxide ion to the vacant site and the transport of the two electrons of the F-center to the new vacant site. For some diffusive jumps, we discovered that the migration barrier is lowered when the two electrons of the F-center form a triplet state (net spin $= 2\mu_B$) at the saddle point (see the Supplemental Material[11] for a snapshot of the simulation cell). In evaluating the overall oxygen diffusivity, we used the lowest migration barriers found for V_O^x along each direction.

Fully ionizing the F-center leads to the formation of $V_O^{\bullet\bullet}$. For the shortest diffusive jumps (along ⟨100⟩ and ⟨001⟩), the migration barrier of $V_O^{\bullet\bullet}$ is significantly less than that of V_O^x. This is consistent with a common trend identified for the diffusion of F-center in oxides[20] and was explained by the columbic repulsion between the localized electrons and the oxide ion during the hop of V_O^x.

The interstitial O_i'' occupies the octahedral site in the conventional unit cell, eightfold coordinated by lattice oxygens.[2] We found the migration barrier for the direct diffusive jumps of O_i'' to be very high (>5 eV). Instead, this defect migrates by the interstitialcy mechanism as shown in Fig. 1(b), where the migrating interstitial replaces one lattice oxygen, which is then pushed to the next interstitial site. Because of the tetragonal distortion of the oxygen columns in T-ZrO_2, four of the lattice oxygens that coordinate O_i'' are at a distance of 2.44 Å, and the other four are at 2.10 Å; hence, two distinct interstitialcy migration barriers exist, as shown in Table I. The classical pair potential predictions of Ref. 19 for these two barriers are also shown in Table I and seem to be consistent with our findings.

By combining the migration barriers and the concentrations, we obtained the self-diffusivity of each defect and the total oxygen self-diffusivity D_{tot} as a function of T and P_{O_2}. We consider the range 1500 K $\leq T \leq$ 2300 K, in which T-ZrO_2 is thermodynamically stable without doping. Figure 2(a) and 2(b) is a reproduction of the previously[2] calculated concentrations of all electronic and ionic defects in T-ZrO_2 at 1500 K and 2000 K. Figure 2(c) and 2(d) shows the calculated diffusivities at the same temperatures. Figure 2(c) is at 1500 K and represents the low-T behavior ($T \leq$ 1700 K), while Fig. 2(d) is at 2000 K and represents the high-T behavior. The criterion for this temperature classification is the number of different slopes that log D_{tot} exhibits as a function of log P_{O_2}. For T-ZrO_2 these slopes of log D_{tot} conform mainly to those of log D of $V_O^{\bullet\bullet}$ since this defect predominates within a wide range of T and P_{O_2} [as shown in our recent work[2] and also in Fig. 2(a) and 2(b)] and also has a low migration barrier along ⟨100⟩. The exception is at very low P_{O_2} where the contribution of V_O^x to total diffusivity becomes significant.

The low-T behavior, as in Fig. 2(c), is characterized by two main regimes of P_{O_2}. In the high-P_{O_2} regime, $V_O^{\bullet\bullet}$ is mainly charge-balanced by the zirconium vacancies V_{Zr}'''' (Ref. 2). Hence, log$[V_O^{\bullet\bullet}]$ and consequently log D_{tot} are roughly independent of P_{O_2}, as expected based on the law of mass action combined with the charge neutrality condition ($[V_O^{\bullet\bullet}] \approx 2[V_{Zr}'''']$). In the low-$P_{O_2}$ regime, free electrons charge-balance $V_O^{\bullet\bullet}$ (Ref. 2). Thus, both log$[V_O^{\bullet\bullet}]$ and log D_{tot} exhibit a (−1/6)

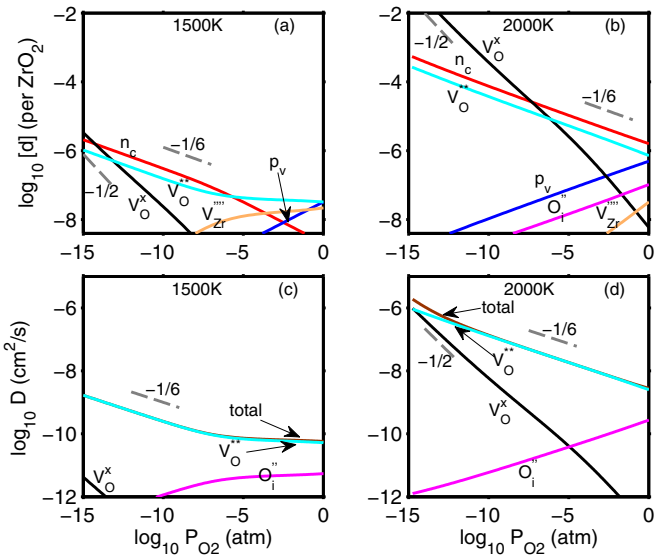

FIG. 2. (Color online) Reproductions of the previously calculated concentrations of electronic and ionic defects at (a) 1500 K and (b) 2000 K from Ref. 2. Zirconium interstitials are not shown for clarity. Ionic defects are denoted by Kröger–Vink notation, whereas n_c an p_v denote conduction band electrons and valence band holes, respectively. Calculated self-diffusivities for oxygen defects and total oxygen self-diffusivity as a function of P_{O_2} at (c) 1500 K and (d) 2000 K.

slope in accordance with the new charge neutrality condition ($2[V_O^{\bullet\bullet}] \approx n_c$) and the law of mass action. At very low P_{O_2}, the (−1/6) slope of log D_{tot} is modified by the contribution of V_O^x. The latter defect is neutral and, except for a small electronic entropy contribution,[2] its concentration is not affected by the charge neutrality condition. It follows that log$[V_O^x]$ always has a (−1/2) slope. In Fig. 2(c), the V_O^x contribution is not shown, as we limited the P_{O_2} axis to 10^{-15} atm to facilitate the comparison with Fig. 2(d). At high temperatures, as in Fig. 2(d), the zero-slope region at high P_{O_2} disappears and the (−1/6) slope for both log$[V_O^{\bullet\bullet}]$ and log D_{tot} dominates for most of P_{O_2} values. At very low P_{O_2}, the contribution of V_O^x to diffusion changes the slope of log D_{tot} to be a weighted average between (−1/6) and (−1/2).

The gradual transition from the low-T to the high-T behavior is illustrated in Fig. 3(a), which depicts the isothermal D_{tot} as a function of P_{O_2}. In order to perform Arrhenius analysis and extract an effective activation barrier, we plot in Fig. 3(b) the isobaric D_{tot} as a function of $1/T$. The hallmark of Fig. 3(b) is the non-Arrhenius behavior on high-P_{O_2} isobars, which do not lend themselves to identifying one effective diffusion barrier over the entire temperature range. The explanation of such non-Arrhenius behavior resides in the different mechanisms of charge neutralization as a function of temperature in T-ZrO_2 introduced above. To rationalize this, imagine an isobaric (e.g., $P_{O_2} = 1$ atm) cooling experiment. At high temperatures ($T >$ 1700 K), $V_O^{\bullet\bullet}$ is charge-balanced by free electrons. Upon cooling, the concentration of $V_O^{\bullet\bullet}$ decreases in an Arrhenius fashion until about 1700 K, below which the charge neutralization mechanism changes to involve

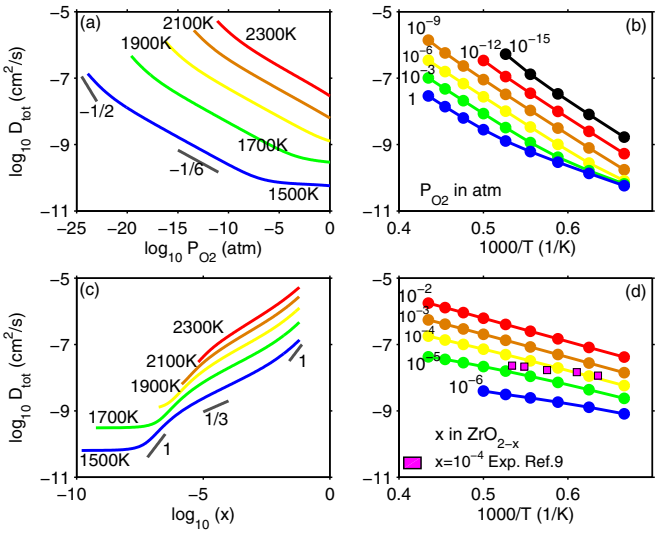

FIG. 3. (Color online) (a) Isothermal oxygen self-diffusivities as a function of P_{O_2}. (b) Isobaric oxygen self-diffusivities as a function of $1/T$. (c) Isothermal oxygen self-diffusivities as a function of the off-stoichiometry x in T-ZrO_{2-x}. (d) Constant off-stoichiometry oxygen self-diffusivities as a function of $1/T$. The experimental data shown in panel (d), adapted from Ref. 9, are self-diffusivities obtained by scaling the measured tracer diffusivities by the appropriate correlation factor (of about 0.65) determined in Ref. 9.

cation vacancies such that $[V_O^{\bullet\bullet}] \approx 2[V_{Zr}^{////}]$. Further cooling continues to decrease $[V_O^{\bullet\bullet}]$ in an Arrhenius fashion but with $(-\partial \log[V_O^{\bullet\bullet}]/\partial(1/T))$ having a value less than the corresponding one at the higher temperatures. This leads to the overall non-Arrhenius behavior over the entire range of temperatures considered here. The low-P_{O_2} isobars, on the other hand, have one charge neutrality mechanism ($2[V_O^{\bullet\bullet}] \approx n_c$) for all temperatures shown, and hence they conform to the Arrhenius behavior.

To the best of our knowledge, the only experiments in the literature to determine oxygen diffusivity in single-crystal undoped T-ZrO_2 were performed at constant off-stoichiometry x by Park and Olander.[9] Maintaining constant off-stoichiometry in the experiments allows probing the migration barrier of the dominant defect that causes the given off-stoichiometry, decoupled from the temperature dependence of the concentration of that defect. To compare with these experiments and to understand the variation of diffusivity with an experimentally accessible quantity x, we plot in Fig. 3(c) the isothermal oxygen diffusivities as a function of x, and in Fig. 3(d) the oxygen diffusivities at constant off-stoichiometry as a function of $1/T$. The experimental data from Ref. 9 are also shown in Fig. 3(d).

Close to stoichiometric composition and at low T where $V_O^{\bullet\bullet}$ is charge-balanced by $V_{Zr}^{////}$, $\log D_{\text{tot}}$ is roughly independent of x [Fig. 3(c)]. This zero slope region is absent at high T. As the degree of off-stoichiometry increases, the slope of $\log D_{\text{tot}}$ increases toward a value of 1 at all temperatures. The value of 1 is what is expected from Eq. (1) when the off-stoichiometry is attributed solely to $V_O^{\bullet\bullet}$ ($x \propto [V_O^{\bullet\bullet}]$), which is approximately the case when $V_O^{\bullet\bullet}$ is the predominant ionic defect and simultaneously neutralized by free electrons. By continuous deviation from stoichiometry on an isotherm, the slope of $\log D_{\text{tot}}$ decreases toward a value of $1/3$. In this range of x, V_O^x predominates concentration-wise, but diffusion is still mainly due to $V_O^{\bullet\bullet}$ because of its much lower migration barrier (see Table I). Thus, the predomination of V_O^x leads to the proportionality relation $x \propto [V_O^x] \propto P_{O_2}^{-1/2}$, and the fact that $V_O^{\bullet\bullet}$ controls the total oxygen diffusivity leads to $D_{\text{tot}} \propto [V_O^{\bullet\bullet}] \propto P_{O_2}^{-1/6}$. Combining these two proportionalities produces $D_{\text{tot}} \propto x^{1/3}$, explaining the $1/3$ slope. Beyond the $1/3$ region, further departure from stoichiometry results in a monotonic increase of the slope of $\log D_{\text{tot}}$ toward a value of 1, indicating that $[V_O^x]$ reaches to values high enough to surpass the impact of the low migration barrier of $V_O^{\bullet\bullet}$; hence, self-diffusion is dominated by V_O^x.

In the experiments of Ref. 9 shown in Fig. 3(d), P_{O_2} was adjusted at each temperature to achieve a stoichiometric composition of T-ZrO_2. However, the inevitable presence of aliovalent cationic impurities in the samples leads to off-stoichiometric composition by $x = 10^{-4}$, as determined in Ref. 9 using atomic absorption spectroscopy. The level of quantitative agreement in our calculated diffusivity in pure T-ZrO_{2-x} at $x = 10^{-4}$ and the measured values in the impurity-containing samples is reasonable.

On the other hand, the experimental data in Fig. 3(d) exhibit a much lower effective barrier of 0.58 eV compared with the effective barrier of 1.27 eV from our simulation results at $x = 10^{-4}$. Much of this discrepancy can be understood by observing that the oxygen vacancy defects in experiments and our simulations are not entirely the same. In the experiments, the 10^{-4} off-stoichiometry is solely due to $V_O^{\bullet\bullet}$, which is needed to charge-balance the aliovalent impurity cations, whereas in the simulation of pure, undoped T-ZrO_{2-x}, the off-stoichiometry is due to both $V_O^{\bullet\bullet}$ and V_O^x. Based on our calculated migration barriers in Table I and assuming that all the 10^{-4} off-stoichiometry is by virtue of $V_O^{\bullet\bullet}$, we obtain and effective barrier of 0.40 eV, closer to the experimentally observed barrier of 0.58 eV. The remaining 0.18 eV discrepancy can be, in part, attributed to the binding of the positively charged $V_O^{\bullet\bullet}$ to the negatively charged acceptor cations present in the experiments. This binding can increase the migration barrier of $V_O^{\bullet\bullet}$. However, it is not possible to preclude the uncertainties in the experiments and the approximations in the calculations, which definitely can contribute to the discrepancy. At the end of this paper, we provide a summary of possible improvements in the theoretical prediction of self-diffusivity.

Using the filled circles in Fig. 3(b) and 3(d) (or similar ones for the isobars and constant x lines not shown), we fit the isobaric and constant off-stoichiometry diffusivities to the Arrhenius relation $D_{\text{tot}} = D_0 \exp(-E_{\text{eff}}/k_B T)$. Thus, we obtained an effective activation barrier E_{eff} and a prefactor D_0 as a function of P_{O_2} in Fig. 4(a) and as a function of x in Fig. 4(b). For the non-Arrhenius isobars, we fit a single activation barrier and prefactor to facilitate comparison with the Arrhenius isobars.

A diffusion barrier evaluated at constant P_{O_2} [Fig. 4(a)] represents both the formation and the migration of the defects.

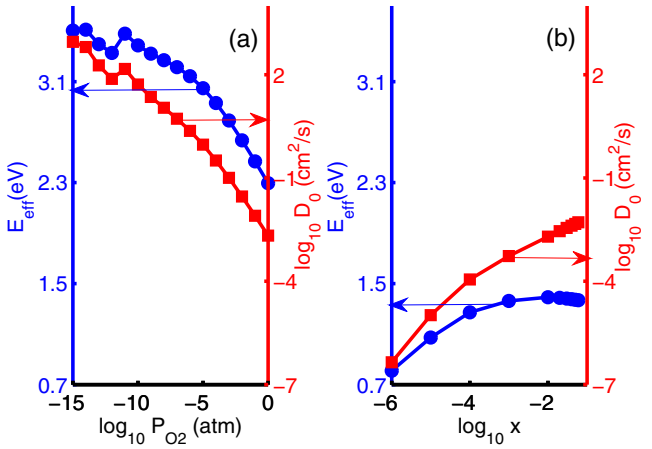

FIG. 4. (Color online) The effective activation barrier E_{eff} (blue circles) and effective prefactor D_0 (red squares) for oxygen diffusion in T-ZrO_{2-x} as a function of (a) P_{O_2} and (b) x.

As P_{O_2} decreases, the oxygen chemical potential decreases, the chemical potential of electrons (Fermi level) increases,[2] and $[V_O^x]$ gradually dominates over $[V_O^{\bullet\bullet}]$. The first factor decreases the formation energy of both vacancies, the second increases the formation energy of $V_O^{\bullet\bullet}$, and the last factor increases the average migration barrier for oxygen. The second and third factors win, and we observe in Fig. 4(a) an increase in the effective activation barrier as P_{O_2} decreases. Moreover, the non-Arrhenius behavior on the high-P_{O_2} isobars is reflected in the figure by lowering the effective barrier at high P_{O_2} more than would be expected by extrapolating from low P_{O_2}.

On the other hand, a diffusion barrier evaluated at constant x [Fig. 4(b)] represents primarily the migration barriers of the defects. Since oxygen in T-ZrO_2 diffuses mainly through $V_O^{\bullet\bullet}$ and V_O^x, the effective diffusion barrier at constant x is a weighted average of the migration barriers of these two defects. Close to stoichiometric compositions, $V_O^{\bullet\bullet}$ is predominant, and the effective diffusion barrier is relatively low, as in Fig. 4(b). By continuous departure from stoichiometry, V_O^x gradually predominates, and the effective diffusion barrier consequently increases until it reaches about 1.4 eV, conforming to the lowest migration barriers for V_O^x. Ironically in Fig. 4(a) and 4(b), the highest values for oxygen diffusivity are coincident with the highest activation barriers, emphasizing the importance of the prefactor (affected by the defect concentration) in deciding the magnitude of the overall diffusivity.

Before concluding, we envisage some refinements and extensions for the approach presented here to predict self-diffusion in metal oxides. First, we used the harmonic approximation to sample the phonons' contribution to the free energy of formation of the defects.[2] However, at elevated temperatures, phonon-phonon interaction and thermal expansion can impact both the defect formation and migration.[5,21] These effects are currently expensive computationally to consider for a material with a band gap, such as ZrO_2 here. But with the increase of computational capabilities, it is essential to examine their contribution to self-diffusion. Second, the model system used here, tetragonal ZrO_2, does not exhibit significant departure from stoichiometry until very low P_{O_2}, indicating the adequacy of the approximation of noninteracting defects for most of the P_{O_2} range examined. However, many other metal oxides easily reduce or oxidize with slight variations of P_{O_2} around atmospheric pressure, and for these oxides, defect-defect interactions are sizable. This situation is amenable to theoretical treatment using a cluster expansion Hamiltonian combined with Monte Carlo simulations.[22] Third, in this paper the jump frequency Γ_k^d was computed using the harmonic transition state theory with the migration entropy implicitly accounted for through the attempt frequency term υ_k^d. It is possible to explicitly account for the migration entropy by evaluating the vibrational frequencies at the saddle point and the initial state. This computation is expensive and typically does not lead to significant quantitative corrections for diffusive jumps in the bulk of a crystalline solid. More important is the formalism of transition state theory that assumes no return jumps across the saddle point and for which the system does not retain a memory of the failed jump attempts. These assumptions might break down at the highest temperatures considered here, and in particular for the lowest migration barriers such as that of O_i''. More advanced treatments[23] of this situation can be applied to remedy this deficiency of transition state theory. Finally, it is also possible to improve the accuracy of the electronic structure calculations by adopting hybrid functionals or higher rungs on the Jacob ladder.[24]

IV. CONCLUSION

We presented a framework based on random-walk diffusion theory to predict self-diffusion in metal oxides, informed by first principles–based calculations of defect formation and migration energies. We demonstrated the approach on oxygen diffusion in tetragonal zirconia and validated our results with prior experimental results. Defect concentrations evaluated through charge neutrality condition are combined with defect mobilities within the random-walk diffusion theory. The resultant self-diffusivity is, as expected, a function of two independent thermodynamic variables, either (T, P_{O_2}) or (T, x). Performing Arrhenius analysis on isobaric or constant x diffusivities yields a spectrum of activation barriers and prefactors. We believe that the systematic analysis presented here can reconcile the scatter in the measured self-diffusion activation barriers in many metal oxides, such as the 1.9–3.3 eV scatter for zinc diffusion in ZnO (Refs. 4,25) or the 0.9–1.3 eV for oxygen diffusion in UO_2.[26]

ACKNOWLEDGMENTS

This research was supported by the Consortium for Advanced Simulation of Light Water Reactors (CASL), an Energy Innovation Hub for Modeling and Simulation of Nuclear Reactors under US Department of Energy Contract No. DE-AC05-00OR22725. We acknowledge the National Science Foundation for computational support through the XSEDE Science Gateways program with the research allocation (TG-DMR120025). Atomistic visualizations were generated using the software VESTA.[27]

*Corresponding author: byildiz@mit.edu

[1]H. Tuller and S. Bishop, Annu. Rev. Mater. Res. **41**, 269 (2011); A. Kushima and B. Yildiz, J. Mater. Chem. **20**, 4809 (2010); A. Chroneos, B. Yildiz, A. Tarancón, D. Parfitt, and J. Kilner, Energy and Environ. Sci **4**, 2774 (2011).

[2]M. Youssef and B. Yildiz, Phys. Rev. B **86**, 144109 (2012).

[3]Y.-M. Chiang , D. P. Birnie, and W. D. Kingery, *Physical Ceramics: Principles for Ceramic Science and Engineering* (John Wiley & Sons, New York, 1997).

[4]A. Janotti and C. G. Van de Walle, Phys. Rev. B **76**, 165202 (2007).

[5]J. H. Harding, Rep. Prog. Phys. **53**, 1403 (1990).

[6]P. Erhart and K. Albe, Phys. Rev. B **73**, 115207 (2006).

[7]G. E. Murch, in *Diffusion in Crystalline Solids*, edited by G. E. Murch and A. S. Nowick (Academic Press, Orlando, 1984).

[8]G. Roma, Y. Limoge, and S. Baroni, Phys. Rev. Lett. **86**, 4564 (2001).

[9]K. Park and D. R. Olander, J. Electrochem. Soc. **138**, 1154 (1991).

[10]G. H. Vineyard, J. Phys. Chem. Solids **3**, 121 (1957).

[11]See Supplemental Material at http://link.aps.org/supplemental/10.1103/PhysRevB.89.024105 for the values of the multiplicities and the projections, a comparison between the conventional and primitive cells, and the triplet state at the saddle point for the neutral vacancy jump.

[12]G. Henkelman, B. P. Uberuaga, and H. Jónsson, J. Chem. Phys. **113**, 9901 (2000).

[13]G. Kresse and D. Joubert, Phys. Rev. B **59**, 1758 (1999).

[14]G. Kresse and J. Hafner, Phys. Rev. B **47**, 558 (1993); **49**, 14251 (1994); G. Kresse and J. Furthmüller, Comput. Mater. Sci. **6**, 15 (1996); Phys. Rev. B **54**, 11169 (1996).

[15]J. P. Perdew, K. Burke, and M. Ernzerhof, Phys. Rev. Lett. **77**, 3865 (1996); **78**, 1396 (1997).

[16]D. W. McComb, Phys. Rev. B **54**, 7094 (1996).

[17]P. Kofstad and D. J. Ruzicka, J. Electrochem. Soc. **110**, 181 (1963).

[18]A. Eichler, Phys. Rev. B **64**, 174103 (2001).

[19]Xian-Ming Bai, Yongfeng Zhang, and Michael R. Tonks, Phys. Chem. Chem. Phys. **15**, 19438 (2013).

[20]A. L. Shluger, A. Foster, J. L. Gavartin, and P. V. Sushko, in *Nano and Giga Challenges in Microelectronics*, edited by J. Greer, A. Korkin, and J. Labanowski (Elsevier, Amsterdam, 2003).

[21]B. Grabowski, T. Hickel, and J. Neugebauer, Phys. Status Solidi (b) **248**, 1295 (2011).

[22]C. B. Gopal and A. van de Walle, Phys. Rev. B **86**, 134117 (2012).

[23]K. J. Laidler, *Chemical Kinetics*, 3rd ed. (Prentice Hall, New York, 1987).

[24]J. P. Perdew, MRS Bull. **38**, 743 (2013).

[25]A. Janotti and C. G. Van de Walle, Rep. Prog. Phys. **72**, 126501 (2009).

[26]D. A. Andersson, T. Watanabe, C. Deo, and B. P. Uberuaga, Phys. Rev. B **80**, 060101(R) (2009).

[27]K. Momma and F. Izumi, J. Appl. Crystallogr. **44**, 1272 (2011).